Theory of orbital moment collapse under pressure in FeI_2

J. Kuneš,[1,2] H. Rosner,[1,3] Deepa Kasinathan,[1] C. O. Rodriguez,[4] and W. E. Pickett[1]
[1]*Department of Physics, University of California, Davis, California 95616, USA*
[2]*Institute of Physics, AS CR, Cukrovarnická 10, 162 58 Praha 6, Czech Republic*
[3]*Max Planck Institute for Chemical Physics of Solids, D-01187 Dresden, Germany*
[4]*IFLYSIB, Grupo de Física del Slido, CC 565, La Plata 1900, Argentina*
(Received 7 February 2003; revised manuscript received 14 April 2003)

FeI_2 is an insulating antiferromagnet with an unusual magnetic structure at ambient pressure. Recently, hyperfine field, electric field gradient, and other local quantities at the Fe site were measured over a wide range of pressures indicating a collapse of the orbital magnetic moment below the insulator-to-metal transition. In the present work we apply local density approximation (LDA) and LDA+U approaches to calculate the electronic structure and to investigate the Fe on-site quantities. We propose that the vanishing of the orbital moment is connected to the change of orbital order as reflected in the symmetry of the occupied minority-spin orbital. We find good agreement between the calculated and measured hyperfine fields and quadrupolar shifts, and make predictions which can serve to validate the proposed mechanism of orbital moment collapse experimentally.

DOI: 10.1103/PhysRevB.68.1151XX PACS number(s): 71.28.+d, 75.50.Ee, 75.30.−m

I. INTRODUCTION

The origin and character of magnetic moments and their interactions in insulators, and the understanding of the resulting behavior, remain a very active area of study because of discoveries of new and unexpected types of magnetic behavior. For magnetic ordering, the dimension and the connectivity of the magnetic lattice are exceedingly important, and often small relative changes of exchange couplings swing the balance from one type of order to another or sometimes to lack of order (spin liquid behavior). For describing the origin and characteristics of the local moment, which is composed of both a spin and an orbital part and is dependent on the environment, recent developments in theoretical techniques have proved to be important. We discuss some of them below.

There are many different classes of magnetic insulators, and each presents its own specific behavior and accompanying theoretical questions. The layered transition-metal dihalides have been of interest for decades as good realizations of model magnetic systems with important questions about exchange coupling and field-induced metamagnetic transitions; $FeCl_2$ and $FeBr_2$ have been studied particularly closely for these reasons. The magnetic behavior of the compound FeI_2 presents a conundrum. The iron dihalide structure type is simple, consisting of a hexagonal layered CdI_2 structure ($P\bar{3}m1$ space group, No. 164 in the International Tables) characteristic of many transition-metal dihalides (NiI_2, $FeCl_2$, etc.). The hexagonal layer of Fe cations is sandwiched (I-Fe-I) by a similar (but displaced) layer of I above and below, with Fe-I layer spacing such that the Fe ion is nearly perfectly octahedrally coordinated with six I anions at ambient pressure. The structure, in which the layers are van der Walls bonded, is shown in Fig. 1.

The magnetic arrangement is more complex than other transition-metal halides, however, and is sensitive to pressure. $FeCl_2$ and $FeBr_2$, for example, have a simple antiferromagnetic (AFM) ground state composed of FM layers whose spin direction alternates from layer to layer. Applying a magnetic field results in a metamagnetic transition to a saturated FM phase. For FeI_2, Gelard *et al.*[1] reported an AFM onset at 9.3 K. More interestingly, the spin alignment within a layer is AFM, composed of alternating zigzag chains of aligned moments. In the layer above, this arrangement has been shifted by one atom along the chain and also one atom perpendicular to the direction of the chains, and the net repeat distance is four layers. The spin direction is along the hexagonal axis; in fact, a strong uniaxial anisotropy coefficient $D=26$ K was established early on by Fujiata *et al.*[2]

Neutron scattering in the presence of an applied field by Wiedenmann *et al.*[3,4] revealed unexpected behavior, in light

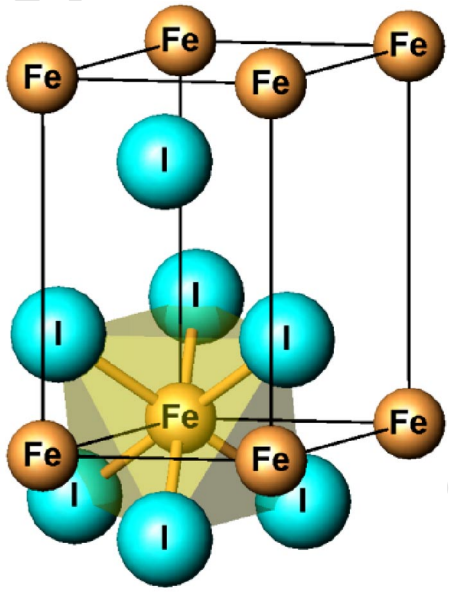

FIG. 1. Crystal structure of FeI_2, showing the hexagonal I-Fe-I sandwich layers. FeI_6 octahedron is shown to indicate the orientation, which has one face perpendicular to the hexagonal c axis.

of the simpler behavior of other ferrous halides mentioned above. For applied fields along $\hat{c}$ up to 13 T, four other phases occur, separated by first-order phase boundaries. These phases include, besides the commensurate phase described above, ferrimagnetic, noncollinear (triple $\vec{k}$ type), and a disordered but correlated phase, before the saturated FM is reached. This complex phase diagram reflects the occurrence of competing tendencies involving many exchange couplings, in spite of the fact that only short-range coupling might have been anticipated. Wiedenmann *et al.* obtained a set of three intraplanar and two interplanar exchange couplings that could account for the phase diagram. Tanaka and Uryu[5,6] have also considered what is necessary to account for the magnetic behavior of FeI_2, obtaining a somewhat different picture and even considering three-spin and four-spin couplings.

Pasternak and co-workers[7,8] have reported several characteristics of the evolution of FeI_2 under pressure. At 20 GPa, after a volume decrease of $\sim 30\%$ ($\Delta c/c \sim -0.2, \Delta a/a \sim -0.1$) a sluggish isostructural volume collapse to a high-pressure (HP) phase begins. This transition results from a discontinuous change in c and is accompanied by metallization and loss of the Fe moment. However, around 17–18 GPa an electronic transition to an intermediate pressure (IP) phase is observable as a discontinuous change in the Fe hyperfine field H_{hf} and electric field gradient which does not show up in the lattice parameters.[7] For pressure in the 17–20 GPa range[7] (i.e., in the IP phase) the magnetic structure simplifies, with the Fe spins within a layer aligned, but alternating layers antialigned into a simple AFM structure. The spins, however, lie at a 35° angle with respect to the hexagonal a axis, and $T_N \approx 260$ K, 25 times higher than the ambient pressure value. Pasternak *et al.* argue that the electronic transition at 17 GPa signals the loss of the orbital magnetic moment on Fe while it remains an antiferromagnetic insulator, the first such transition ever observed. The 20 GPa transition (electronic + magnetic + structural + volume collapse) marks a Mott or charge transfer transition.

FeI_2 thus displays a set of characteristics that makes it unique among magnetic insulators. The hexagonal layers of Fe might be expected to have an AFM tendency, but the triangular lattice frustrates simple nearest-neighbor AFM order. Superexchange via the I anion is one candidate for exchange coupling, but the I^- ion is less polarizable than the more usual O^{2-} ion and the Fe-I-Fe angle is near 90°, making the coupling small in magnitude and indeterminate in sign. Direct interatomic Fe-Fe exchange is another route to exchange coupling. Both mechanisms are volume dependent, and under pressure the Fe layer becomes FM (as occurs in the other dihalides at ambient pressure). Then, an electronic insulator - metal transition occurs with 5% volume collapse and loss of magnetism, in a material which is a wide-gap insulator at ambient pressure.

Recently Youn, Sahu, and Kim have reported electronic structure studies[9] of $FeBr_2$, concentrating on the magnetic moment of the Fe ion and changes due to correlation effects. They found that correlation corrections (discussed below) were necessary to obtain an insulating state and that when such corrections were included there was relatively little hybridization between the Fe $3d$ states and the Br $4p$ valence states.

To date there has been no attempt to understand the electronic structure, magnetic coupling, and the volume collapse transition in FeI_2 from electronic structure calculations. In this paper we use accurate full-potential band structure methods to obtain the electronic and magnetic structures predicted by density functional theory, within both the local density approximation (LDA) and its extension for systems that contain atoms where the on-site Coulomb repulsion is particularly important (LDA+U).

II. METHOD OF CALCULATION

Full-potential linearized augmented-plane-waves (FLAPW's) as implemented in WIEN2k code (Ref. 10) and its LDA+U (Ref. 11) extension were used. The s, p, and d states were treated using the APW+lo scheme,[12] while the standard LAPW expansion was used for higher l's. Local orbitals were added to describe Fe $3p$ and I $4d$ and $5s$ states. The basis size was determined by the criterion $R_{mt}K_{max} = 8.0$, atomic sphere radii being $2.3a_0$ for Fe and $2.45a_0$ for I. Spin-orbit coupling as well as the additional LDA+U potential were included self-consistently in the second variational step.[13] The cutoff energy for the second variation was set approximately 2.3 Ry above the edge of the valence band. The Brillouin zone was sampled with regular mesh containing 50 irreducible k points. The convergence of the quantities of interest with respect to the number of k points as well as to the basis size was checked. The LDA functional of Perdew and Wang[14] and the LDA+U with the double-counting term of Anisimov *et al.*[15] were used. If not stated otherwise, the magnetization was constrained to the c-axis direction.

III. RESULTS OF CALCULATIONS

A. LDA electronic structure

It is of interest to understand first the electronic structure of FeI_2 before the Fe ion is allowed to become magnetic or strong correlation effects are included. The d^6 configuration of Fe^{2+} and the nearly octahedral symmetry of the local environment suggest that the $3d$ states will be split by a substantial crystal field Δ_{cf}; nevertheless, all majority states are occupied, leaving only one of the minority t_{2g} states to be occupied. Thus the exchange splitting $\Delta_{ex} > \Delta_{cf}$. The LDA result (see Fig. 2) is that each of the t_{2g} and e_g bandwidths is 0.6 eV, and the crystal field splitting of the centroids of these bands is about 0.6 eV. A small gap of ~ 60 meV results, separating these two band complexes. All of these states lie within a 4-eV energy gap, with the mean $3d$ energy lying about 1.2 eV above the valence band maximum.

Allowing FM order, FeI_2 becomes half-metallic with the $d^5\uparrow$, $d^1\downarrow$ configuration of the Fe d shell, lowering the total energy by ~ 1.2 eV. The half-metallicity guarantees the spin moment per unit cell to be integral ($4\mu_B$). Almost 90% of the spin moment resides on the Fe site ($3.5\mu_B$ within the Fe sphere) and the rest is distributed on the I sites. Hence there

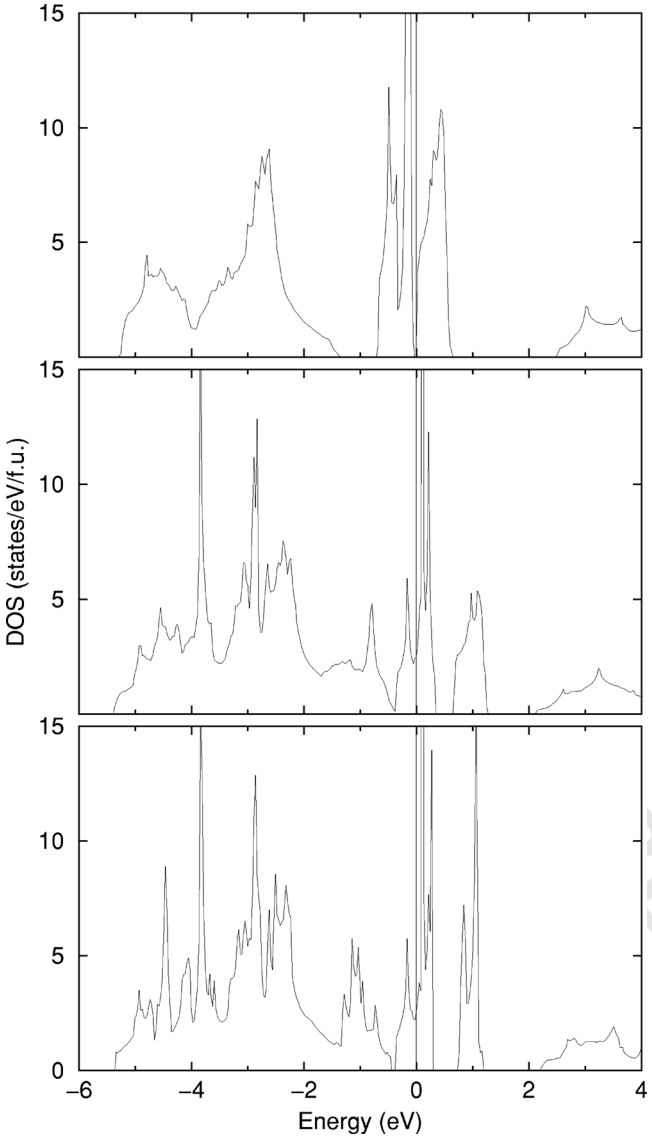

FIG. 2. Total densities of states as obtained with the LDA exchange-correlation functional for different magnetic states: paramagnetic (upper panel), ferromagnetic (middle panel), and antiferromagnetic (bottom panel) in the c direction.

is significant magnetic polarization of the I^{-1} ions. Spin-orbit coupling induces an orbital moment of $0.19\mu_B$ on Fe and $0.01\mu_B$ on I. Since the majority-spin d band is completely filled, it is the symmetry of the occupied minority-spin d orbital which governs the on-site physical properties, such as orbital moment, hyperfine field, or electric field gradient. Below, mechanisms underlying splitting of the d band are investigated in order to understand this symmetry.

Nearly octahedral coordination with the neighboring iodines makes e_g-t_{2g} splitting a dominant feature of the d band, as shown in Fig. 3. While the electrostatic crystal field results in t_{2g} states lying below the e_g's, reversal of this order for the majority spin suggests the I p–Fe d hybridization to be the origin of the splitting. Sizable bumps of the e_g density of states (DOS) within the p manifold visible in both spin channels point to p-e_g hybridization, while no such feature is observed for the t_{2g} DOS, thus exhibiting negligible p-t_{2g} hybridization. Consequently the e_g states are shifted upwards or downwards depending on whether they lie above or below the I p states, while the position of t_{2g} bands is independent of their position relative to the I p states.

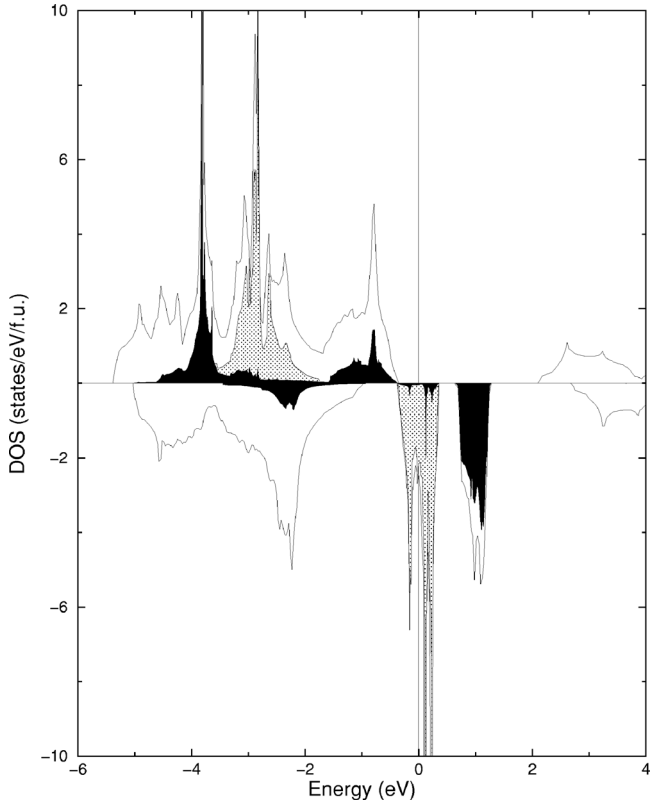

FIG. 3. Spin-resolved density of state for the LDA ferromagnetic solution at low pressure. The shaded areas denote Fe d projected densities with e_g (solid line) and t_{2g} (dotted line) symmetry.

Another interesting question is the origin of the t_{2g} splitting into an a_g singlet and e_g' doublet. There are two candidates: (i) deviation of the nearest-neighbor octahedron from the regular one characterized by the separation of Fe and I layers and (ii) the effect of the farther environment, which lacks the octahedral symmetry, supposedly dominated by hybridization within the Fe layer. Both these mechanisms break local symmetry of the Fe site in the same way. In order to identify the leading mechanism calculations for different Fe-I layers separation where performed. Finding only marginal changes of the a_g-e_g' splitting pattern, we conclude that the in-plane hybridization is the origin of the splitting.

Finally, we performed calculations for two artificial antiferromagnetic structures corresponding to simplest possible in-plane and out-of-plane arrangements. In both cases we found the density of states deviating from the ferromagnetic one only marginally. The electric field gradients and magnetic moments were also consistent with the ferromagnetic ones, indicating a weak influence of the magnetic order on the on-site properties.

B. LDA+U ferromagnetic electronic structure

To account for the strong on-site Coulomb repulsion that splits occupied and unoccupied states, we have applied the

LDA+U method with $U=5.44$ eV and $J=0.95$ eV. These values are representative of those used for the Fe cation in other magnetic insulators (see, e.g., Ref. 16). The main effect is to split one occupied orbital out of the minority t_{2g} manifold leading to an insulating ground state. The studied quantities should not be very sensitive to the particular values of U and J, mostly because the t_{2g} states hybridize only weakly with the valence I p states. With respect to the chosen double-counting scheme[15] we point out that the studied system falls well into the fully localized limit as is demonstrated by its strong insulating character and the orbital occupation numbers shown below.

The main objective of the LDA+U calculations was to understand the on-site properties (magnetic moments, electric field gradient, and hyperfine field) observed in the insulating phase at low and intermediate pressures. In order to facilitate a detailed study we confined ourselves to the ferromagnetic structure assuming that it provides on-site quantities relevant for the experimentally observed antiferromagnetic structure. We used two different sets of experimental lattice parameters: $a=3.9514$ Å, $c=6.2486$ Å corresponding to 2.7 GPa and $a=3.5989$ Å, $c=5.7200$ Å corresponding to 19.4 GPa in the low-pressure (LP) phase of Ref. 8. Additional calculation was performed for the structure denoted as 19.4 GPa IP in Ref. 8, yielding similar values of the studied quantities as the 19.4 GPa LP structure.

C. LDA+U at ambient pressure

The primary effect of applying the LDA+U method is to separate the occupied and unoccupied states with a gap of the order of U and to favor integral occupation of the orbitals (see Fig. 4). Since the character and orientation of the occupied minority-spin d orbital is crucial for the on-site quantities, we performed a search for self-consistent solutions starting from different occupation matrices. It turned out that an occupied e_g state does not lead to a self-consistent solution, due to the strong p-e_g hybridization, which prevents the e_g state from lying near the I $5p$ energy. This is in agreement with an LDA calculation yielding the t_{2g} symmetry of the occupied state. Starting from a $t_{2g}\rightarrow a_g+e_g'$ symmetry of the occupied orbital we obtained three different self-consistent solutions. The orbital occupation numbers, obtained by diagonalization of the occupation matrix, are much the same in all of them, amounting to 0.15 electron in each of the two e_g states and 0.92 in one of the t_{2g}-derived states, the remaining two t_{2g}'s being unoccupied. The small but non-negligible e_g occupation is enforced by the substantial $pd\sigma$ hybridization and may have important physical effects. The partial occupation of the e_g states results from mixing with the occupied I p states.

The three solutions can be characterized as follows.

(A) Two solutions consist of one electron occupying the e_g' orbitals. Taking the hexagonal c axis for the quantization axis, they can be characterized as real combinations of $Y_{2,2}$ and $Y_{2,-1}$ (solution 1, which we call Hund's rule) or $Y_{2,-2}$ and $Y_{2,1}$ (solution 2, referred to as anti-Hund's rule) spherical harmonics. Approximately they are the time inversion images of each other with only spin-orbit coupling distinguishing them. In agreement with the third Hund's rule, solution 1, which yields the orbital moment of $0.72\mu_B$ (parallel to spin moment), has lower energy than solution 2 with orbital moment of $-0.48\mu_B$ (antiparallel to spin moment).

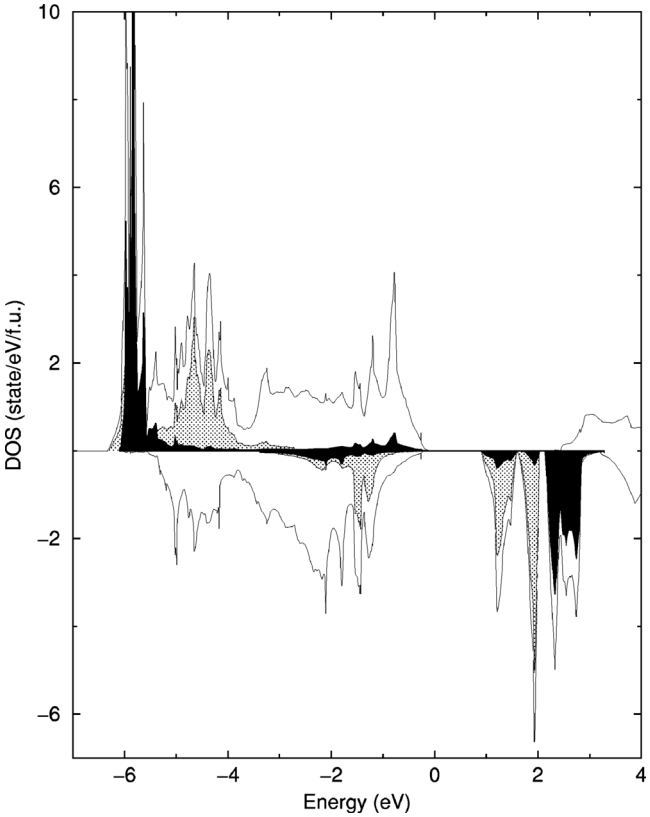

FIG. 4. The same as Fig. 3, except obtained with the LDA+U method.

(B) The third solution has an occupied a_g orbital; i.e., the state has pure $Y_{2,0}$ character. A nearly vanishing orbital moment of $0.04\mu_B$ originates from slight orbital polarization of the partially occupied e_g orbitals.

Since solutions 1 and 2 are distinguished only by the spin-orbit coupling, while the charge and spin distributions are almost the same, it is evident that solution 1 is energetically more favorable at any pressure. Further on we consider primarily solution 1 and refer to it as e_g'. On the other hand, solution 3, referred to as a_g further on, has a very different charge and spin distribution (see Fig. 5). Therefore a change of the structure induced by pressure can lead to reversing of the energies in favor of a_g solution, resulting in collapse of the orbital moment. This is what we refer to as a change of orbital order (strictly speaking orbital order with propagation vector $q=0$). The Fe d projected densities of states corresponding to a_g and e_g' solutions are shown in Fig. 6. The occupied orbital exhibits almost pure a_g or e_g' character. Minor occupation of e_g orbitals arises from Fe-I hybridization.

All of these three solutions retain the symmetry of the lattice for the charge density and potential. To investigate the possibility of spontaneous symmetry breaking, several calculations starting from occupation matrices with lower symmetry were performed. However, self-consistency led to one of the above solutions in all cases. We also performed one

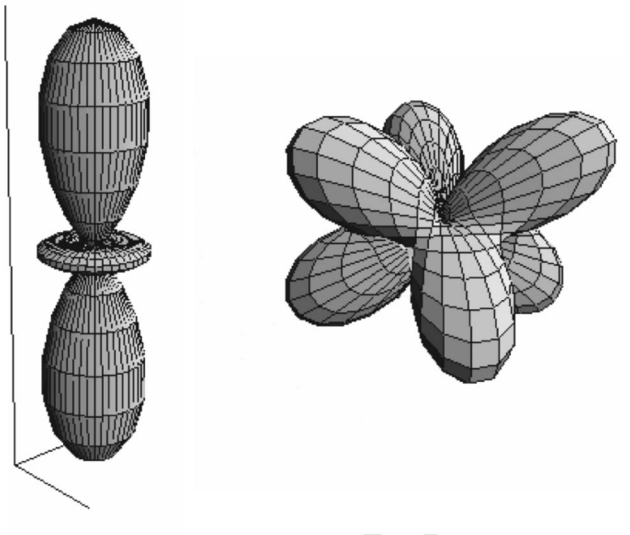

FIG. 5. Angular part of charge distribution $|\psi(\theta,\phi)|^2$ of the a_g (left) and e_g' (right) orbital. The vertical axis coincides with the hexagonal c axis.

LDA+U calculation for the simplest possible in-plane antiferromagnetic order. We obtained antiferromagnetic solutions with all three above-mentioned symmetries yielding Fe magnetic moments and electric field gradients within 2% of their ferromagnetic counterparts.

D. LDA+U total energies

The total energies of a_g and e_g' solutions at 2.7 GPa and 19.4 GPa are shown in Table I. The LDA+U total energy favors the e_g' solution at both pressures, not even indicating a tendency to any transition. However, we argue that this result need not be conclusive.

Experimentally observed collapse of the orbital moment is accompanied by a change of the magnetic structure, consisting in rotation of the magnetization into the ferromagnetic Fe plane while retaining the antiferromagnetic ordering across the planes. Such a transformation is facilitated by a drop of magnetocrystalline anisotropy connected to a vanishing of the orbital moment. The contribution of this process to the total energy is not included in our simplified picture.

However, the energy difference between the two solutions ($\sim$65 meV) is by far too large to be explained by a change of the magnetic structure. We have realized, however, that an incompletely compensated self-interaction in the LDA part of the energy functional results in an error which is of the same order of magnitude. To obtain an estimate of the error, we evaluate the Coulomb self-interaction energy in the occupied orbital for the both solutions. For this purpose we use the formula

$$E_{SI}(\sigma)=\frac{1}{2}\sum_{\substack{m_1,m_2\\m_3,m_4}}\langle m_1,m_3|V_{ee}|m_2,m_4\rangle n_{m_1m_2}(\sigma)n_{m_3m_4}(\sigma), \tag{1}$$

where $n_{mm'}(\sigma)$ is the occupation matrix corresponding to orbital σ and for the matrix element of the Coulomb interaction we use the U-J parametrization. The self-energy difference for the two orbitals, $E_{SI}(a_g)-E_{SI}(e_g')=(3.108-2.985)$ eV$=123$ meV, arises from the nonspherical terms in Eq. (1). The self-interaction energy is larger for the a_g orbital (see Fig. 5). Thus any correction should lower the energy of the a_g solution more than that of e_g'. These arguments show that the possibility of the pressure-induced transition between e_g' and a_g states cannot be ruled out on the basis of LDA+U total energies.

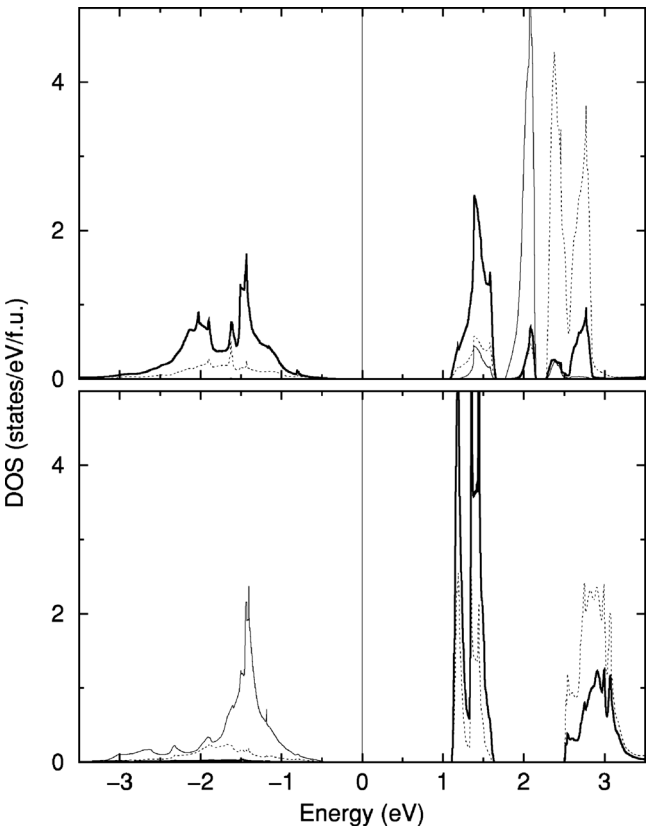

FIG. 6. Detail of the Fe d minority-spin densities of states obtained with the LDA+U method for the e_g' (upper panel) and a_g (lower panel) solutions. Different symmetries of the states are denoted as follows: e_g', thick solid line; a_g, solid line; and e_g, dotted line.

E. Electric field gradients and hyperfine fields

The experimentally observed quadrupolar shift reflects the quadrupole-quadrupole interaction of the nucleus and the

TABLE I. Total energies obtained with LDA+U method for the different self-consistent solutions for low- and intermediate-pressure structures. The calculated equilibrium spacing of Fe and I layers (fraction of the c lattice constant) is shown in the right column. The same values were obtained for the two solutions.

	E_{tot} (Ry)		u
	e_g'	a_g	
2.7 GPa	−30 994.2207	−30 994.2156	0.250
19.4 GPa	−30 994.1258	−30 994.1212	0.273

TABLE II. Electric field gradients at the Fe site obtained with the LDA+U method.

	EFG (10^{21} V m^{-2})	
	e_g'	a_g
2.7 GPa	6.1	−17.5
19.4 GPa	5.6	−16.3

surrounding electron cloud, which can be written in terms of the nuclear quadrupolar moment Q and the gradient V_{zz} of the electric field produced by electrons at the position of nucleus. We use the value $Q=0.15$ b for the quadrupole moment of the Fe nucleus established in Refs. 17 and 18. The electric field gradient (EFG) reflects the deviation of the electron charge distribution from cubic symmetry. In the case of FeI_2 the dominant contribution comes from the single-occupied minority-spin d orbital, the charge density of which is strongly noncubic.

The calculated values of the EFG at the Fe site are shown in Table II. In order to compare these results with experiment, we use the following formula to express EFG's in terms of the Doppler shift:

$$\Delta_D=\frac{cQ}{2E_\gamma}V_{zz}. \tag{2}$$

Using $E_\gamma=14.4$ keV for the energy of γ rays one arrives at the relation

$$\Delta_D[\mathrm{mm\,s^{-1}}]=0.156\times V_{zz}\ [10^{21}\ \mathrm{V\,m^{-2}}]. \tag{3}$$

The calculated quadrupole shift for the e_g' solution ranges from $\Delta_D=0.87$ mm s^{-1} at 19.4 GPa to 0.95 mm s^{-1} at 2.7 GPa. The experimental values are in the range from 0.7 to 0.85 mm s^{-1}, exhibiting a nonmonotonic pressure dependence with a minimum at both the low- and high-pressure ends of the interval. We remark that the value of the EFG obtained with the LDA is 3 times smaller, reflecting the LDA tendency to a more uniform occupation of the d orbitals.

The EFG reflects the nonsphericity of the density, which for this Fe^{2+} ion is due to the occupied minority d orbital. The EFG is almost 3 times larger for the a_g solution than for the e_g' solution, a large difference that can be understood as follows. The a_g orbital is purely $Y_{2,0}\propto 3z^2-1$ (with respect to the c axis), which is the most nonspherical a d orbital can be. The e_g' solution consists of a real combination of $Y_{2,-2}$ and $Y_{2,1}$:

$$\psi_{e_g'}(\theta,\phi)\approx 0.67Y_{2,2}(\theta,\phi)+0.74Y_{2,-1}(\theta,\phi). \tag{4}$$

The coefficients standing by the spherical harmonics are obtained by diagonalization of the occupation matrix and taking the eigenvector with the largest eigenvalue (0.92 in this case). The a_g orbital has 100% t_{2g} character, while the e_g' orbital has 98.8% t_{2g} character. Both orbitals are pictured in Fig. 5. The e_g' density distribution is essentially oblate, while the a_g density distribution is prolate.

Unlike in the low-pressure (orbital unquenched) phase, in the intermediate-pressure (orbital quenched) phase the EFG cannot be measured directly using Mössbauer spectroscopy because of the magnetization tilting.[7] Upon heating above the magnetic ordering temperature only the EFG corresponding to low-pressure phase was detected; i.e., there can be only one type of orbital order in the paramagnetic state. This fact would be consistent with the scenario of the orbital order change if the two types of orbital order exist only in the magnetically ordered state. Such an interpretation is not unrealistic since the orbital moment quenching is accompanied by a change of the magnetic order, suggesting a coupling between the orbital and magnetic order. Although we cannot provide verification of the orbital order change scenario on the basis of total energy calculations, below we make a prediction of the in-field behavior of the hyperfine field which can be compared to future experiment.

The hyperfine field (magnetic field at the nucleus) can be expressed as a sum of four contributions: (1) the contact term arising from the nonzero spin density at the nucleus, (2) the dipolar magnetic field produced by the on-site spin density, (3) the orbital term (the magnetic field produced by the current flowing around the nucleus and proportional to the orbital moment), and (4) the lattice contribution, which is a dipolar field originating from the moments on the other lat-

TABLE III. Hyperfine field at the Fe site as obtained with the LDA+U method. The contributions of the contact, spin dipolar, and orbital term are shown separately. The results denoted a_g^* correspond to occupied a_g orbital with tilted magnetization. The values in brackets were obtained with the modified SIC potential for the core states (only the contact term is modified).

		H_{hf} (T)		
		e_g'	a_g	a_g^*
2.7 GPa	H_{cont}	−17.8 (−29.8)	−17.4 (−29.5)	−17.4 (−29.5)
	H_{dip}	−5.5	15.3	−3.9
	H_{orb}	44.0	1.4	1.2
	H_{tot}	20.7 (8.7)	−0.7 (−12.8)	−20.1 (−32.2)
19.4 GPa	H_{cont}	−12.7 (−24.5)	−12.1 (−24.0)	−12.1 (−24.0)
	H_{dip}	−5.8	14.1	−3.7
	H_{orb}	50.0	1.9	1.4
	H_{tot}	31.5 (19.7)	3.9 (−8.0)	−14.4 (−26.3)

tice sites. The largest contribution to the contact field originates from polarization of the core states. The LDA and related schemes are known to systematically underestimate this contribution.[19,20] In the present work we neglect the lattice contribution, which is typically small in ferromagnets and will be even smaller in an antiferromagnet.

In Table III the total hyperfine field and the different contributions are summarized. The third column, a_g^*, corresponds to an a_g solution with magnetization tilted to 55° with respect to the c axis (experimentally observed magnetic structure), obtained from the a_g solution by rotating the spin moment and adding the spin-orbit coupling in a single cycle only. The orientation of the in-plane component of magnetization is not known experimentally. Since the a_g orbital, whose contribution dominates the spin dipolar term, has full rotational symmetry along the c axis, the spin dipolar term is determined uniquely by specifying the angle between magnetization and the c axis. While the spin density is the same for a_g and a_g^*, yielding the same contact field, the spin dipolar term even changes its sign. Qualitatively this can be understood as follows. With magnetization along the c axis the a_g orbital is prolate with respect to the magnetization direction, yielding a positive dipolar field, while with tilted magnetization the a_g orbital is oblate with respect to the magnetization direction, yielding a negative dipolar field. The residual orbital contribution in the a_g solutions originates from the e_g states, marginally occupied due to hybridization with I p states.

The experimentally observed behavior of the hyperfine field shows a monotonic increase from 7 T to 13 T in the 2.7–19.4 GPa pressure range, followed by jump to 32 T attributed to vanishing of the orbital moment. The LDA+U hyperfine field does not show such a trend, which can be attributed to the well-established underestimation of the contact term. Note that the core functions are basically the same in the LDA+U approach. In order to facilitate comparison with experiment we adopt two ways to surpass this deficiency.

Recently, we have implemented and tested on several compounds the form of self-interaction correction (SIC) proposed by Lundin and Eriksson[21] applied to the core states, yielding systematic improvement of the contact fields.[22] Since this method is not well established yet, we also present estimates of the contact field based on the empirical correction of Coehoorn[20] amounting to $-4.2\ \mathrm{T}\times m_s[\mu_B]$ for $3d$ elements. For the Fe spin moment ranging from $3.4\mu_B$ to $3.5\mu_B$ at higher and lower pressure we obtain a correction of about -14.5 T, resulting in contact fields of -27 T and -32 T for higher and lower pressure, respectively. These numbers agree rather well with those obtained with the self-interaction correction for the core states shown in Table III. Taking the correction of the contact field into account we obtain a fair agreement with the experimental data.

The experimental hyperfine field in the low-pressure phase varies monotonously from 7 to 13 T. The calculated field exhibits an increase from 8.7 to 20 T, which arises partially from an increase of the orbital moment and partially from a decrease of the contact term having an opposite sign. Vanishing of the orbital term in the a_g solution results in an almost 50 T drop of the hyperfine field to -26.3 T, which agrees with experimentally observed 30 T (note that the sign of the field is not measured in the experiment). Comparison of hyperfine fields for the a_g solution with orientations of the magnetization reveals a rather large variation of the spin dipolar term resulting from the strongly nonspherical shape of the a_g orbital. Facilitated by the experimentally observed decrease of magnetocrystalline anisotropy it opens an interesting possibility for experimental verification of the proposed scenario. Applying an external magnetic field along the c axis, we expect a variation of the hyperfine field with the angle between the local moments and the c axis from 26.3 T, for tilted magnetic structure, to 8 T, for parallel-to-c orientation.

IV. CONCLUSIONS

We have presented a comprehensive numerical study of the single ion properties of Fe^{2+} ion in FeI_2. Using the LDA+U method with the values of U and J generally accepted for this type of material we obtained an insulating ground state in agreement with experiment. As our investigation was focused on the on-site physical characteristics, we assumed the ferromagnetic ground state to provide a reasonable description. We checked this assumption, performing a calculation for an antiferromagnetic structure, although the magnetic order along the c axis was not precisely the experimental one. Our main objective was to understand the experimentally observed jump of the hyperfine field around 18 GPa interpreted as a vanishing of the orbital moment. Obtaining LDA+U solutions with both sizable ($0.72\mu_B$) and negligible orbital moment, we infer that the vanishing of the orbital moment originates from a pressure-induced change of the symmetry of the occupied minority-spin d orbital.

At low pressure the twofold-degenerate (if spin-orbit coupling is not considered) e_g' orbitals are occupied by a single minority-spin electron. The electronic transition around 19 GPa is associated with a change to a_g occupation and loss of the orbital moment. Estimating the error connected with the uncompensated self-interaction in the LDA part of the LDA+U functional, we come to a conclusion that such a transition takes place on an energy scale beyond the resolution of the LDA+U method. We have obtained the electric field gradient on the Fe site, which is in good agreement with the experimental data available for the low-pressure phase. Employing a modified SIC scheme for the core states we have obtained Fe hyperfine fields consistent with the empirical correction of the LDA data proposed by Coehoorn.[20] Thus corrected hyperfine fields correspond well to the experimental ones in both low- and intermediate-pressure phases.

Furthermore, we provide predictions for quantities not yet measured. We have calculated the electric field gradient in the intermediate phase to be almost 3 times larger than in the low-pressure phase. We furthermore predict a rather strong dependence of the hyperfine field on the angle between the local moments and the hexagonal c axis.

ACKNOWLEDGMENTS

We are grateful to M. P. Pasternak for communication of Ref. 8 before publication. We acknowledge helpful discussions with P. Novák. This work was supported by National Science Foundation Grant Nos. DMR-0114818 and DGE-0209264 and by the Deutscher Akademischer Austauschdienst.

[1] J. Gelard, A.R. Fert, P. Meriel, and Y. Allain, Solid State Commun. **14**, 187 (1974).
[2] T. Fujiata, A. Ito, and K. Ono, J. Phys. Soc. Jpn. **21**, 1734 (1966).
[3] A. Wiedenmann, L.P. Regnault, P. Burlet, J. Rossat-Mignotd, O. Kounndé, and D. Billerey, J. Magn. Magn. Mater. **74**, 7 (1988).
[4] A. Wiedenmann, L.P. Regnault, P. Burlet, J. Rossat-Mignotd, O. Kounndé, and D. Billerey, Physica B **156&157**, 305 (1989).
[5] Y. Tanaka and N. Uryu, J. Phys. Soc. Jpn. **40**, 404 (1976).
[6] Y. Tanaka and N. Uryu, J. Phys. Soc. Jpn. **43**, 1569 (1977).
[7] M.P. Pasternak, W.M. Xu, G.K. Rozenberg, R.D. Taylor, G.R. Hearne, and E. Sterer, Phys. Rev. B **65**, 035106 (2001).
[8] G.K. Rozenberg, M.P. Pasternak, W.M. Xu, L.S. Dubrovinsky, J.M.O. Guillén, R. Ahuja, B. Johansson, and T.L. Bihan, Phys. Rev. B (to be published).
[9] S.J. Youn, B.R. Sahu, and K.S. Kim, Phys. Rev. B **65**, 052415 (2002).
[10] P. Blaha, K. Schwarz, G.K.H. Madsen, D. Kvasnicka, and J. Luitz, Computer code WIEN2k, An Augmented Plane Wave + Local Orbitals Program for Calculating Crystal Properties, Karlheinz Schwarz, Techn. Universität Wien, Wien, 2001.
[11] P. Novák, F. Boucher, P. Gressier, P. Blaha, and K. Schwarz, Phys. Rev. B **63**, 235114 (2001).
[12] E. Sjöstedt, L. Nordström, and D.J. Singh, Solid State Commun. **114**, 15 (2000).
[13] A.B. Shick, A.I. Liechtenstein, and W.E. Pickett, Phys. Rev. B **60**, 10 763 (1999).
[14] J.P. Perdew and Y. Wang, Phys. Rev. B **45**, 13 244 (1992).
[15] V.I. Anisimov, I.V. Solovyev, M.A. Korotin, M.T. Czyzyk, and G.A. Sawatzky, Phys. Rev. B **48**, 16 929 (1993).
[16] I.I. Mazin and V.I. Anisimov, Phys. Rev. B **55**, 12 822 (1997).
[17] G. Martínez-Pinedo, P. Schwerdtfeger, E. Caurier, K. Langanke, W. Nazarewicz, and T. Söhnel, Phys. Rev. Lett. **87**, 062701 (2001).
[18] P. Dufek, P. Blaha, and K. Schwarz, Phys. Rev. Lett. **75**, 3545 (1995).
[19] S. Blügel, H. Akai, R. Zeller, and P.H. Dederichs, Phys. Rev. B **35**, 3271 (1987).
[20] R. Coehoorn, J. Magn. Magn. Mater. **159**, 55 (1996).
[21] U. Lundin and O. Eriksson, Int. J. Quantum Chem. **81**, 247 (2001).
[22] P. Novák, J. Kuneš, Wei Ku, W.E. Pickett, and F. Wagner, Phys. Rev. B (to be published).

PROOF COPY [BB8980] 025335PRB